Electromagnetic (EM) Design of an Annular Coupled Accelerating Structure for the Advanced Compact Carbon Ion Linac (ACCIL)

Yuchen Han
Department of Physics, Cornell University

Brahim Mustapha
Physics Division, Argonne National Laboratory
(Dated: August 12, 2018)

Radiotherapy with carbon ion beams has become a popular topic throughout the world, due to its desirable features including sharp Bragg peak and greater radio-biological effectiveness. the Argonne National Laboratory recently embarks on developing the Advanced Compact Carbon Ion Linac, a linear accelerator designed for performing carbon therapy. The work presented here focuses on the coupled cavity linac (CCL) of ACCIL, which is crucial for its compactness. In this project, we designed the CCL based on the annular coupled structure and successfully optimized the cavity frequency and field distribution. We also studied the sensitivity of the cavity to machining errors and the tuning capabilities of tuners installed on the accelerating cells. Lastly, we applied the coupled resonator model to describe our accelerating cavity.

I. INTRODUCTION

Recently, there is a strong interest worldwide in using carbon ion beams for radiotherapy [1]. Carbon ion beams have a sharp Bragg peak (Figure 1), which is desirable for more localized cancer treatment and reduced toxicity to healthy cells. Carbon ion beams also have a greater radio-biological effectiveness (RBE), allowing the treatment of more 'radio-resistant' tumors. [2]
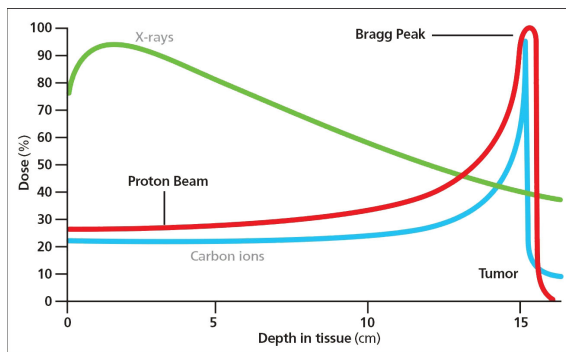

FIG. 1. Comparison of the energy deposition as a function of depths for x-rays, proton beams and carbon ion beams.

On the other hand, existing carbon therapy facilities around the world are all based on synchrotron technologies, which are less suitable for delivering high quality beams with variable energies and more space-consuming compared to linear accelerators (linacs) [3]. Therefore, Argonne National Laboratory embarks on the development of a linac-based carbon ion therapy facility, known as the Advanced Compact Carbon Ion Linac (ACCIL) (Figure 2)

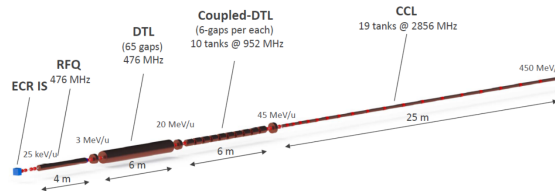To make ACCIL compact, a high gradient needs

FIG. 2. Schematic diagram of the different sections of ACCIL

to be achieved in the last part of the accelerator, i.e., the coupled cavity linac (CCL). Several accelerating structures have been proposed [2], one of them being the annular coupled structure (ACS) (Figure 3), a standing wave $\pi/2$-mode accelerating cavity structure.An advantage of ACS is that it is relatively compact by design, as the coupling cells are placed off-axis thus do not increase the length of the cavity. It is also robust to small manufacturing imperfections, as the operating mode is the $\pi/2$-mode instead of the π-mode [4].
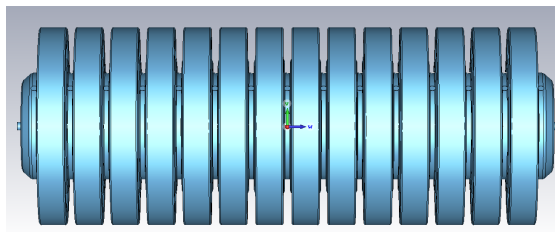

FIG. 3. 3D model of the ACS cavity consisting of 15 accelerating cells and 14 coupling cells.

In this project, we designed a 15-cell accelerat-

ing cavity based on an existing ACS structure and optimized it to the desired frequency of 2856 MHz and a flat electric field distribution along the central axis where the beam passes through. We also studied the effect on the frequency and field flatness caused by small errors in the geometry of the cavity and the tuning capabilities of the tuners installed on the accelerating cells. The commercial software CST Microwave Studio is used extensively to obtain the mode frequencies and field distributions. Finally, we attempted to use a theoretical model, the coupled resonator model, to describe our cavity.

II. OPTIMIZATION

The optimization phase entails two main aspects, namely the resonant frequency and the field distribution. We also present some selected design and radio-frequency (RF) parameters of the optimized final structure.

A. Frequency

We started from the ACS structure in the J-PARC project in Japan, which is designed for a lower frequency of 972 MHz [5]. To bring the frequency to 2856 MHz, we varied the cell radius. This is because the electromagnetic mode in every accelerating cell is TM_{01} [4], and the frequency of this mode for an equivalent pillbox cavity is given by

$$f_0 = 2.405 \times \frac{c}{2\pi R} \qquad (1)$$

where R is the cell radius [4]. With numerical simulations conducted in CST Studio, we obtained the optimum cell radius R = 38.853 mm.
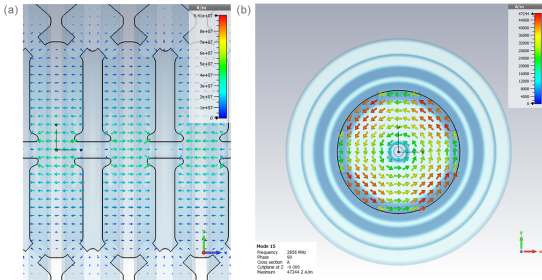

FIG. 4. Electric [(a) left view] and magnetic [(b) front view] field in an accelerating cell, showing that the EM mode in each cell is TM01. The 4 coupling windows (located on the x- and y-axes in our coordinate system) break the axial symmetry of the magnetic field.

B. Field Flatness

As the cavity is not infinitely periodic, the electric field distribution is not uniform when all the accelerating cells have the same geometry. To obtain a flat field while not complicating the manufacturing process too much, we kept the geometry of the middle cells the same while only varying a few parameters of the two end cells.

Through literature review and numerical simulations with CST, we found that the cell gap and coupling window length are good parameters to tune for a uniformly distributed field [6].

The optimum combination of these parameters is: cell gap = 0.4096 × drift tube length, and coupling window length = 28.17 mm (Figure 5 (a)).Compared to the middle cells, the percentage differences in these parameters are -18.08% and +1.514% respectively. This gives us a very flat field, as seen in (Figure 5 (b)) where the magnitude of the peaks of E_z in all cells have very close values.
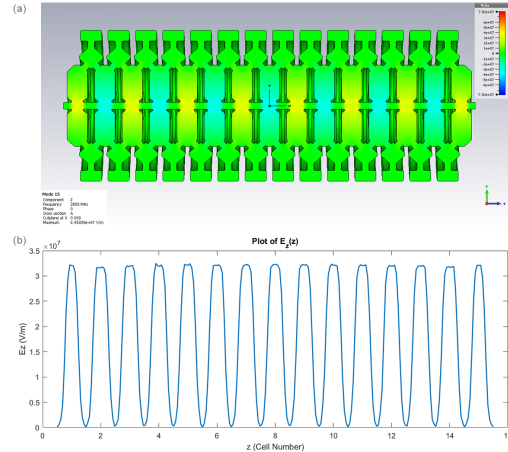

FIG. 5. Plot of $E_z(z)$ in the structure (a) and along the central axis of the cavity (b)

To quantify the field flatness, we define the variance of the peak E_z-field between cells (E_{peak}) to be

$$\sigma^2 = \sum_{n=1}^{15} \left(\frac{E_{peak} - \bar{E}_{peak}}{\bar{E}_{peak}} \right) \qquad (2)$$

In the case of the ideal geometry, the value is calculated to be $\sigma^2 = 4.1060 \times 10^{-4}$

C. Radio-Frequency Parameters

Some common RF parameters are shown in the table below (Figure 6).

Selected RF Parameters	Values
Frequency	2856 MHz
Peak Electric Field	7.92394×10^7 V/m
Peak Magnetic Field	7.97734×10^4 A/m
Shunt Impedance	1.79156×10^7 V/m
Q-Factor	9.04229×10^3

FIG. 6. Selected RF parameters of the optimized accelerating cavity

III. SENSITIVITY AND TUNING

As real-life machining is never exact, we want to look into how imperfections in the cell geometry affects the frequency and field distribution in the cavity, and whether we can bring them back to near-ideal with tuners installed on the accelerating cells.

A. Sensitivity Analysis

Assuming a machining precision of $\pm 25 \mu m$ [7], we studied the effect of errors in the radius of accelerating cells on the resonant frequency (Figure 7 (a)) and field flatness in the cavity (Figure 7 (b) (c)). From these plots of response functions, we can see that an increased radius in any accelerating cell causes the frequency of the cavity to increase, and vice versa.This is expected from the dependence of the TM_{01} mode frequency expression. Therefore, the maximum frequency variation occurs when all cells have the maximum error in the same direction, thus giving us a frequency range of 2854.09 MHz (when the errors on all cells are $+25$ μm) to 2857.88 MHz (when the errors on all cells are -25 μm).

As for the field distribution, an increase in cell radius concentrates the electric field. The color plot shows that an increase in the radius of the middle few cells (cell 7 - 9) only causes a slight increase in the electric field, which is largely confined to a region near itself, while an error in cells near the ends results in a greater change in the electric field distribution and creates a field gradient in the entire cavity, causing an opposite change in the field distribution on the other side of the cavity.
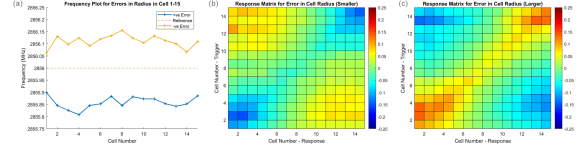

FIG. 7. Plot of responses of resonant frequencies and electric field distributions in the presence of geometry errors in the accelerating cells. (a) Resonant frequencies when the radius of each cell is given an error of $\pm 25 \mu m$. (b) Field distribution response when there is a $+25 \mu m$ error in a cell (vertical-axis). Color represents the fractional change in peak E_z in each cell (horizontal axis). For example, the pixel in row 1 column 2 represents the fractional change in peak E_z in cell 2 when there is a $+25 \mu m$ error in cell 1. (c) Same as (b) except the error in cell radius is $-25 \mu m$.

B. Tuning Capabilities

To ensure that the above-mentioned perturbations in frequency and field flatness can be corrected even after the cavity is built, tuners need to be installed on the accelerating cells. Here, for simplicity, we model the tuners as small cylinders that create dents or bumps on the accelerating cells. These tuners are placed 45° from the coupling windows, as these are the positions where the magnetic field is the strongest, thus can cause the greatest change in the cavity frequency and field distribution (Figure 8).
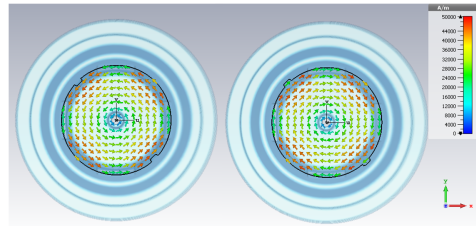

FIG. 8. Models of tuners pushing in (left) and pulling out (right) on the accelerating cell wall, and the associated magnetic field in the cell.

We first simulated with two tuners on each cell, which each have a radius of 3.2 mm and a maximum tuning depth of 2 mm in both in and out directions. The tuning range with two tuners is from 2855.03 MHz (when all tuners are pulled out by 2 mm) to 2859.47 MHz (when all tuners are pushed in by 2 mm).

To give the tuners a sufficient tuning range to correct the frequency perturbations, 4 tuner need be installed on each cell. We again found the response functions for the tuning effect on each cell (Figure

9). This gives a tuning range of 2853.85 MHz to 2863.11 MHz, which is sufficient for our purpose.
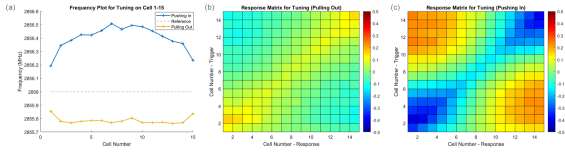

FIG. 9. Plot of responses of resonant frequencies and electric field distributions when pushing or pulling 4 tuners installed on each accelerating cell. The interpretation is similar to Figure 7. Note that the colorbar range is doubled compared to previous plots to show the full range.

Note that the decrease in frequency when tuners are pulled out is significantly less than the increase in frequency when the tuners are pushed in. This might be a limitation of our modeling, as a cylindrical hole on the accelerating cells perturbs the magnetic field less than the mechanical distortion on the shape of the cell created by an actual tuner. More realistic mechanical simulation on tuner distortions on the shape of the cells could be done in the future.

C. Optimization of A Cavity with Random Errors in Cell Radii

To demonstrate that the tuners are indeed capable of correcting the frequency and field distribution, we modeled a 15-cell cavity with a random error in radii on each cell in the range of $[-25, +25]\mu m$, generated by MATLAB (Figure 11). This gives a perturbed frequency of 2855.485 MHz and a large field variance of 0.2014 (Figure 10, blue curve)
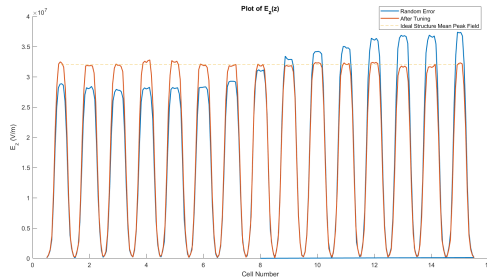

FIG. 10. Electric field distribution for the structure, with random errors in cell radius (blue curve), and after tuning (orange curve).

We then adjusted the tuners on a few cells to get back a frequency of 2856.00 MHz and a reasonably flat field distribution. (Figure 10, orange curve) The configuration of the tuners is given in (Figure 11).

Cell No.	1	2	3	4	5	6	7	8	9	10	11	12	13	14	15
Error/μm	16	20	-19	21	7	-20	-11	2	23	23	-17	24	23	-1	15
Tune/mm	0.5	0.5	0	0	0	0	-0.5	0	1.0	0	0	0	1.1	0	0

FIG. 11. Random error on cell radii and tuner configuration that tunes the randomly perturbed cavity back to the desired frequency and flat field.

The tuning is partly based on response functions we obtained in the previous section, but the process is far from systematic. A future projects could look into developing a detailed and more systematic tuning algorithm based on the perturbed frequency and field distribution, as well as the response functions.

IV. COUPLED RESONATOR MODEL

A useful model to describe an accelerating cavity consisting of a chain of periodic cells is the coupled resonator model [8].
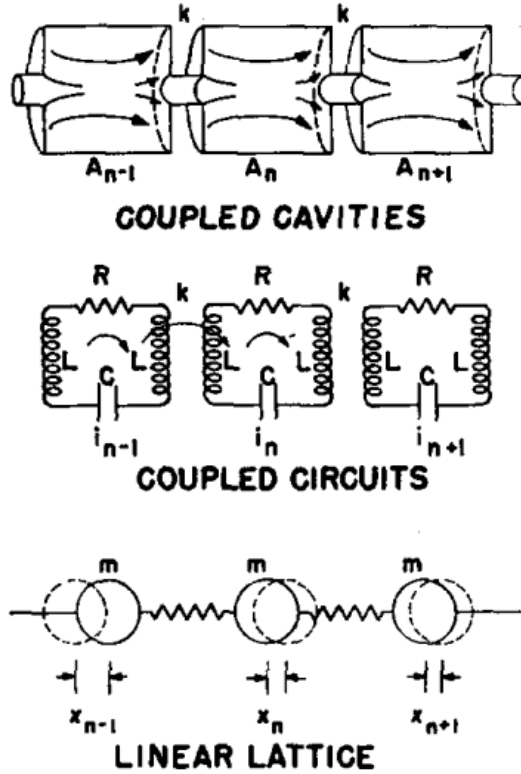

FIG. 12. Analogy among coupled cavities, coupled circuits and linear lattice. Figure from [4]

As each cell has its resistance, inductance and capacitance, we can draw a parallel between an accelerating cavity and a chain of RLC circuits (Figure 12), taking into account the parameters including individual cell resonant frequency f_0, quality factor Q, and coupling coefficient k between adjacent cells [8] .

In our case, as the accelerating and coupling cells have very different geometries, the chain of resonator is biperiodic instead of simply periodic, thus we need to consider the frequencies of both types of cells. Since there is also non-trivial second nearest cell coupling, between accelerating and coupling cells respectively, two additional parameters need be included into the model. Besides, as the simulation is done under the PEC assumption, the quality factor Q is very large, thus the terms involving $\frac{1}{Q}$ can be safely ignored. Therefore, we have to define 5 parameters to describe the system, namely the accelerating and coupling cell resonant frequencies f_a, f_c, nearest neighbor coupling coefficient k_1, and second nearest neighbor coupling coefficients k_a, k_c, between accelerating cells and coupling cells respectively. This gives us an expression for the dispersion relation [8]:

$$k_1^2 \cos^2 \phi = (1 - \frac{f_a^2}{f^2} + k_a \cos 2\phi)(1 - \frac{f_c^2}{f^2} + k_c \cos 2\phi)$$

(3)

where $\phi = \frac{\pi q}{2N}$, $q = 0, 1, 2, ...2N$ and N being the total number of unit cells, which is equivalent to the total number of accelerating cells (the two half-cells at the ends count as one full accelerating cell).

The five parameters can be obtained by performing two parametric studies with a 'unit cell' of the structure consisting of a full coupling cell sandwiched between two half-accelerating cells with PEC termination (Figure 13 (a)). Similar to that in [9] and [10], varied f_a by changing the accelerating cell radius (Figure 13 (b)), and varied f_c by changing the height of the coupling cell gap (Figure. 13 (c)), and obtained the frequencies of the three relevant modes with simulations in CST Studio. By plotting the quantities $x = F_-^{-2} + F_+^{-2}$ against $y = (F_-^{-2} - F_+^{-2})^2$, we can obtain y_{min} and the associated x value x_{min}. These quantities, together with the $\pi/2$ mode frequency, can give us a system of 6 equations, which can be used to solve for the 5 unknown parameters stated above.

$$\frac{1}{F_0^2} = \frac{1 - k_a}{f_a^2}$$

(4)

$$\tilde{f_a}^{-2} = \frac{1}{2}(y_{min} + x_{min}^2)/x^{min}$$

(5)

$$k_1^2 = \frac{1}{2}(1 + k_c)f_a\frac{y_{min}}{x_{min}}$$

(6)

$$\frac{1}{F_0^2} = \frac{1 - k_c}{f_c^2}$$

(7)

$$\tilde{f_c}^{-2} = \frac{1}{2}(y_{min} + x_{min}^2)/x^{min}$$

(8)

$$k_1^2 = \frac{1}{2}(1 + k_a)f_c\frac{y_{min}}{x_{min}}$$

(9)

where $\tilde{f_a}^2 = \frac{f_a^2}{1+k_a}$, and $\tilde{f_c}^2 = \frac{f_c^2}{1+k_c}$.

Solving the above system of equations gives

$$f_a = 2871.29$$
$$f_c = 2834.88$$
$$k_a = -0.01074$$
$$k_c = 0.01473$$
$$k_1 = (0.06611 + 0.06138)/2$$
$$= 0.06374$$

where k_1 is obtained in two ways so the average of the two results is taken.
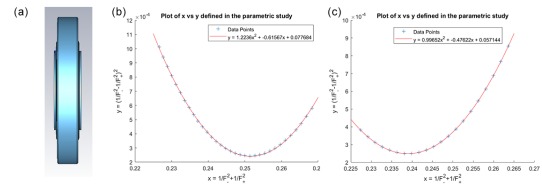

FIG. 13. (a) The unit cell structure used for the parametric study, consisting of a full coupling cell sandwiched between two half-accelerating cells with PEC termination. (b) (c) Plots of $x = F_-^{-2} + F_+^{-2}$ against $y = (F_-^{-2} - F_+^{-2})^2$, as defined in the parametric studies. For (b), the radius of the accelerating cell (b) is varied from 35 mm to 43 mm. For (c), the height of the coupling cell gap (c) is varied from 5 mm to 9 mm.

Using the above parameters, we compared the calculated and simulated dispersion relations for the half-cell termination structures for $N = 1, 2, ...5$ (Figure 14 (a) - (e)). We also compared the calculations results for $N = 14$ against our ideal 15-cell structure with tuned end cells and full cell termination, both of which have the same set of relevant

modes (Figure 14 (f)). The comparison shows that the calculated and simulated data largely agree with each other. Thus, the model indeed captures the general trend of the dispersion relations for all models. However, discrepancy also arises as the model assumes continuity at $\phi = \frac{\pi}{2}$, i.e., the stopband of the structure is closed. On the other hand, the simulated results seem to suggest that there exists a stopband in our structure [8] [4].

On one hand, it shows that the coupled cavity model used does not describe our cavity exactly; on the other hand, we also realize that we might want to perform further tunings to the cavity and close the stopband, due to the potential benefits of improving the mode separation [4]. These are both possible areas for future studies.
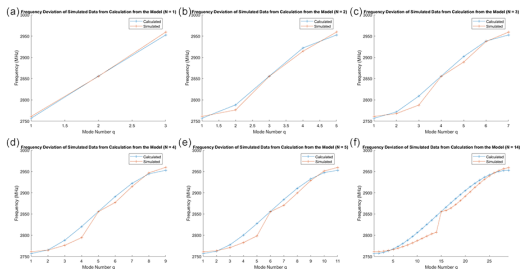

FIG. 14. Comparison between dispersion relations calculated from the coupled resonator model and dispersion relations simulated by CST Studio. (a) - (e) dispersion relations of structures corresponding to N = 1, 2, ... 5 with half-cell terminations. (f) The simulation is done with the optimized 15 cell structure, while the calculation with the coupled resonator model is done for the corresponding N = 14 structure with half-cell terminations on both ends.

V. CONCLUSION AND FUTURE WORK

In this project, we successfully optimized the 15-cell ACS cavity for ACCIL, in which field flatness is achieved by only varying the geometry of the end cells, thus reducing the complexity of production as the middle cells can be mass-produced. We also studied the effect of machining errors on the resonant frequency and the electric field distribution, and verified that such perturbations can be corrected with tuners installed on the accelerating cells. Finally, we attempted to use the coupled resonator model to describe our structure, which captures the general trend of the dispersion relation, but not the feature related to the stopband and the two branches of the passband.

Future projects can look into engineering design and mechanical simulation, such as the exact cell deformation during tuning and its effect on frequency and field flatness. A detailed tuning algorithm can also be developed to automate the tuning process. An improvement on the coupled cavity model can also be made to include the passbands and the stopband into the model, allowing it to describe structures with dispersion relations that are discontinuous at $\phi = \frac{\pi}{2}$, and possibly to use the model to further characterize the perturbation behavior of the cavity. Lastly, further optimization can also be done to explore the possibility of closing the stopband for a better mode separation.

VI. ACKNOWLEDGEMENTS

[1] U.S. Department of Energy. Workshop on ion beam therapy. 01 2013.

[2] Brahim Mustapha. Prospects for a linac-based carbon ion therapy facility in the chicago area. 8 2017.

[3] P N Ostroumov, A Goel, Brahim Mustapha, A Nassiri, Alexander Plastun, Luigi Faillace, Sergey Kutsaev, and Evgeny Savin. Compact carbon ion linac. 10 2016.

[4] T.P. Wangler. *RF Linear Accelerators*. Physics textbook. Wiley, 2008.

[5] N Hayashizaki, H Ao, K Hasegawa, Y Yamazaki, and T Kato. Structure design of the annular coupled structure linac for the jaeri/kek joint project. 08 2018.

[6] R. Wegner P. Ugena Tirado, F. Gerigk. Tuning procedure for the linac4 pi mode structure (pims). 7 2012.

[7] Sergey Kutsaev, R Agustsson, Luigi Faillace, A Goel, Brahim Mustapha, A Nassiri, P Ostroumov, Alexander Plastun, and Evgeny Savin. High gradient accelerating structures for carbon therapy linac. 09 2016.

[8] D. E. Nagle, E. A. Knapp, and B. C. Knapp. Coupled resonator model for standing wave accelerator tanks. *Review of Scientific Instruments*, 38(11):1583–1587, 1967.

[9] V. G. Vaccaro, A. D'Elia, and M. R. Masullo. A rationale to design Side Coupled Linac (SCL): A faster and more reliable tool. *Conf. Proc.*, C060626:1606–1608, 2006. [,1606(2006)].

[10] V. G. Vaccaro A. DElia, M. R. Masullo. An analysis of lumped circuit equation for side coupled linac (scl). *Proceedings of EPAC 2006, Edinburgh, Scotland*, pages 1600–1602, 2006.